

# State-to-State Scattering of Oriented OH

K. Schreel<sup>†</sup> and J. J. ter Meulen\*

Molecular and Laser Physics, University of Nijmegen, P.O. Box 9010, 6500 GL Nijmegen, The Netherlands

Received: March 20, 1997; In Final Form: June 2, 1997<sup>⊗</sup>

Hexapole state selection of OH molecules and subsequent orientation in an electric field is performed to study orientational effects in rotational excitation of OH in molecular collisions. Laser-induced fluorescence spectroscopy of OH is used to determine the orientational probability distribution function and to measure the cross sections for excitation. For the collisionally induced transitions of OH in the rotational ground state the steric asymmetry is determined for collisions with He, Ar, *n*-H<sub>2</sub>, and *p*-H<sub>2</sub> (*n* = normal, *p* = para). The results show that for He excitation is preferential at the H-end of the molecule, whereas for Ar and H<sub>2</sub> a preference for the O-end is shown in transitions to the lowest rotational states.

## 1. Introduction

In a molecular collision, the relative orientation of the molecules with respect to each other can be very decisive for the outcome of the collision process. Since the pioneering work of Toennies<sup>1</sup> and Kramer and Bernstein<sup>2</sup> on molecular orientation, numerous experiments have been reported on the steric dynamics in chemical reactions.<sup>3</sup> For nonreactive inelastic collisions, however, the dependence of the dynamics on the relative molecular orientation has practically not been studied so far. The study of orientation effects in collisionally induced transitions is of importance not only for a better understanding of rotational energy transfer but also for the interpretation of reaction experiments in which the rotational distribution of the reaction products is measured. In studies of rotational energy transfer, state-to-state collision experiments are believed to provide the highest level information about the interaction potential; however, even more detailed information is obtained about the anisotropy of the potential when the measurements are performed with the molecules oriented in specific directions relative to the collision partner.

Orientation of molecules can be obtained using two basically different techniques. One is applying a laser to prepare the molecules in a specific state. When this state is carefully chosen, this will result in an alignment or eventually in an orientation with regard to the polarization of the laser. Normally this technique is applied in bulk gas circumstances, so no cross sections, but rather rate constants, are obtained. The second technique is based on the usage of an electric field to orient the molecules. Two different approaches can be distinguished. For symmetric top molecules having a dipole moment this can be performed by focusing the molecules in an electrostatic hexapole field and subsequently orienting them in a homogeneous electric field. The alternative way is the “brute force” method in which a strong homogeneous electric field is applied, such that the interaction energy between the polar molecule and the electric field is large compared to the rotational energy.<sup>4</sup> The advantage of the “brute force” orientation is the easier feasibility of an experiment, but the major advantage of hexapole orientation is the inherent state selection of the method. In the case of OH, because of the desired state selection, hexapole orientation seems to be the natural choice. Orientation of molecules in a

homogeneous electric field preceded by hexapole state selection has first been demonstrated by Toennies<sup>1</sup> and Kramer and Bernstein.<sup>2</sup> Since then, this technique has grown to maturity and has been used in several collision experiments. An extensive overview of this subject has been given by Harren *et al.*<sup>5</sup>

In this work orientation effects are studied for inelastic collisions of OH molecules in the ground rotational state <sup>2</sup>Π<sub>3/2</sub>, *J* = 3/2 with Ar, He, normal H<sub>2</sub> (*n*-H<sub>2</sub>), and para H<sub>2</sub> (*p*-H<sub>2</sub>). The state-to-state rotational energy transfer of OH in collisions with these molecules has been studied in detail in previous work.<sup>6,7</sup> It was shown that the experimental results are in good agreement with theoretical data obtained from *ab-initio* quantum calculations. The same *ab-initio* potentials can be used to calculate the orientation effects observed in the present work.

As far as we know the experiment of Stolte and co-workers on NO–Ar<sup>8</sup> is the first one on orientational effects in inelastic collisions. They found large steric effects indicating that O-end collisions are most effective in exciting NO to high rotational states, whereas N-end collisions yield less rotational excitation. The OH molecule is similar to NO in so far it also has a <sup>2</sup>Π electronic structure. However, due to the intermediate character of the angular momentum coupling, the OH molecule behaves completely different from NO in inelastic collisions. It will be shown that also strong differences are present with respect to their steric asymmetries in inelastic collisions.

When interpreting the measured orientation dependent cross sections, knowledge of the orientation distribution function is essential. Photodissociation can yield valuable information with regard to the orientation distribution function and has been used in the past to interpret orientational effects.<sup>9</sup> Recently this has been demonstrated very clearly in the ion imaging experiment of Mastenbroek *et al.*<sup>10</sup> In the present experiment a technique is used to investigate the orientation distribution function, as proposed recently for and demonstrated on NO by Van Leuken *et al.*<sup>8</sup> In this technique use is made of the electric-field-induced mixing of the initially selected upper Λ-doublet state with the lower doublet state. This mixing results in the appearance of “forbidden” lines in the laser-induced fluorescence (LIF) spectrum, of which the intensity is a direct measure for the mixing and consequently the orientation of the molecules.

The outline of this paper is as follows. First, a description of the behavior of the OH molecule in an electric field, the resulting orientational effects, and the LIF detection of these effects are given. Then the experimental setup is described and

\* To whom correspondence should be addressed. E-mail: htmeulen@sci.kun.nl.

<sup>†</sup> Present address: Eindhoven University of Technology, P.O. Box 513, 5600 MB Eindhoven, The Netherlands. E-mail: K.R.A.M. Schreel@wtb.tue.nl.

<sup>⊗</sup> Abstract published in *Advance ACS Abstracts*, September 15, 1997.

subsequently the results are presented and discussed. Finally some conclusions will be drawn.

## 2. Orientation and Detection of OH

**2.1. Orientation of OH in an Electric Field.** Molecules having an electric dipole moment  $\mu$  exhibit normally a linear dependence of the Stark energy on the electric field strength. This effect, known as the first-order Stark effect, can be calculated by treating the Stark interaction  $-\vec{\mu}\cdot\vec{E}$  in first-order perturbation theory. This results in the splitting of every  $J$  level in its  $M$  components, with  $M$  defined as the projection of  $J$  on the axis parallel to the electric field and ranging from  $-J, -J+1, \dots, J$ .

Although OH has a rather large permanent dipole moment of 1.668 D,<sup>11</sup> the Stark effect in OH needs a little different treatment. In OH every rotational level is already split by the  $\Lambda$ -doubling, which is caused by the coupling between the end-over-end rotation of the molecule and the total angular momentum of the electrons. For low electric fields this means that a competition takes place between the  $\Lambda$ -doubling and the Stark interaction, leading to a transition region from pure  $\Lambda$ -doubling at zero electric field strength to a linear Stark effect at high electric field strengths. In first order there is no coupling between states of a different rotational level. This holds only for Stark shifts which are much smaller than the rotational spacing. For OH the rotational spacing is very large and the Stark effect in fields of the order of 10 kV/cm is described accurately by neglecting the coupling of different rotational states.

To calculate the orientational effect, we evaluate the matrix elements of the Stark interaction  $-\vec{\mu}\cdot\vec{E}$  on the basis formed by the wave functions of the two  $\Lambda$ -doublet states belonging to each rotational level. For a pure Hund's case (a) coupling scheme, these wave functions are given by the rigid body rotational wave functions together with an electron and spin angular momentum part:

$$\Phi = |\Omega JM\rangle|\Lambda\Sigma\rangle \quad (1)$$

with the explicit expression for the rigid rotor function given by<sup>12</sup>

$$|\Omega JM\rangle = \sqrt{\frac{2J+1}{8\pi^2}} \mathcal{D}_{\Omega M}^J(\alpha\beta\gamma) \quad (2)$$

The  $|\Lambda\Sigma\rangle$  part will be dropped in the rest of the paper since the relevant information of these quantum numbers is contained in the sign of  $\Omega$ . The sign of  $\Omega$  is chosen to be positive when the projection of  $J$  on the internuclear axis is in the same direction as the dipole moment (pointing from the O-end to the H-end), and negative for the reverse case. When symmetrizing these case (a) functions with regard to  $\Omega$ , the following expressions result:

$$\Phi_\epsilon(\Omega, J, M) = \frac{1}{2}\sqrt{2}(|\Omega JM\rangle + \epsilon|-\Omega JM\rangle) \quad (3)$$

where  $\epsilon = \pm 1$  denotes the symmetry. The  $\Omega$  argument of  $\Phi_\epsilon$  is defined to take on only positive values. The states with  $\epsilon = +1$  are also referred to by e-symmetry, the states with  $\epsilon = -1$  by f-symmetry.<sup>13</sup> In OH, due to the  $\Lambda$ -doubling, the degeneracy of the e and f states is lifted, and every rotational state becomes a doublet of which the upper component has f-symmetry and the lower component has e-symmetry.<sup>14</sup> In the  $\Omega = 1/2$  ladder the ordering reverses above  $J = 7/2$ , but that is of less importance for the following.

The OH molecule is best described with an intermediate Hund's coupling case, for which the wave functions can be written as<sup>15</sup>

$$\Psi_\epsilon(\Omega, J, M) = C_1\Phi_\epsilon(1/2, J, M) + C_2\Phi_\epsilon(3/2, J, M) \quad (4)$$

The value of the constants  $C_1$  and  $C_2$  depends on  $\Omega$  and  $J$ , but this will for simplicity be omitted in the notation.

The matrix elements of  $\vec{\mu}\cdot\vec{E}$  between wave functions of different  $\Omega$ ,  $J$ , and  $M$  are zero, and we are left with the diagonalization of the  $2 \times 2$  blocks in the matrix. The matrix elements have the form:

$$M_{ij} = \langle \Psi_{\epsilon_i}(\Omega, J, M) | -\vec{\mu}\cdot\vec{E} | \Psi_{\epsilon_j}(\Omega, J, M) \rangle \quad (5)$$

The term  $\vec{\mu}\cdot\vec{E}$  can be written as  $\tilde{\mu}_0 \mathcal{D}_{00}^{(1)}(\alpha\beta\gamma) E_z$  when  $\tilde{\mu}_0$  is the dipole moment along the internuclear axis and  $\mathcal{D}_{00}^{(1)}(\alpha\beta\gamma)$  the relevant matrix element of the rotation operator for the transition from the space fixed frame to the body fixed frame. The diagonal matrix elements vanish, as follows from symmetry. The off-diagonal matrix elements are, using eq 4, given by

$$\begin{aligned} \langle \Psi_f | \mathcal{D}_{00}^{(1)} | \Psi_e \rangle &= (C_1)^2 \langle \Phi_f(1/2, J, M) | \mathcal{D}_{00}^{(1)} | \Phi_e(1/2, J, M) \rangle + \\ & (C_2)^2 \langle \Phi_f(3/2, J, M) | \mathcal{D}_{00}^{(1)} | \Phi_e(3/2, J, M) \rangle + \\ & C_1 C_2 \langle \Phi_f(1/2, J, M) | \mathcal{D}_{00}^{(1)} | \Phi_e(3/2, J, M) \rangle + \\ & C_1 C_2 \langle \Phi_f(3/2, J, M) | \mathcal{D}_{00}^{(1)} | \Phi_e(1/2, J, M) \rangle \quad (6) \end{aligned}$$

And using eq 3, it follows

$$\begin{aligned} \langle \Psi_f | \mathcal{D}_{00}^{(1)} | \Psi_e \rangle &= \frac{1}{2}(C_1)^2 (\langle 1/2 JM | \mathcal{D}_{00}^{(1)} | 1/2 JM \rangle - \\ & \langle -1/2 JM | \mathcal{D}_{00}^{(1)} | -1/2 JM \rangle) + \frac{1}{2}(C_2)^2 (\langle 3/2 JM | \mathcal{D}_{00}^{(1)} | 3/2 JM \rangle - \\ & \langle -3/2 JM | \mathcal{D}_{00}^{(1)} | -3/2 JM \rangle) \quad (7) \end{aligned}$$

The integrals over  $\mathcal{D}_{00}^{(1)}$  are calculated using eq 2:

$$\begin{aligned} \langle \Omega JM | \mathcal{D}_{00}^{(1)} | \Omega JM \rangle &= \frac{2J+1}{8\pi^2} \int \mathcal{D}_{\Omega M}^{J*} \mathcal{D}_{00}^{(1)} \mathcal{D}_{\Omega M}^J d\Omega \\ &= (2J+1)(-)^{M-\Omega} \begin{pmatrix} J & 1 & J \\ -\Omega & 0 & \Omega \end{pmatrix} \begin{pmatrix} J & 1 & J \\ -M & 0 & M \end{pmatrix} \quad (8) \\ &= \frac{M\Omega}{J(J+1)} \end{aligned}$$

The final result for the matrix element is

$$\begin{aligned} \langle \Psi_f | \mathcal{D}_{00}^{(1)} | \Psi_e \rangle &= \langle \Psi_e | \mathcal{D}_{00}^{(1)} | \Psi_f \rangle \\ &= -\tilde{\mu}_0 E_z \frac{M}{J(J+1)} (1/2(C_1)^2 + 3/2(C_2)^2) \quad (9) \\ &\equiv Q \end{aligned}$$

The shift and splitting in energy due to the Stark effect is then given by the eigenvalues of the  $2 \times 2$  matrix,

$$\begin{vmatrix} \Delta E_\Lambda - \lambda & Q \\ Q & -\lambda \end{vmatrix} = 0 \quad (10)$$

The basis functions are chosen in such a way that the first column is for the upper state ( $\Psi_f$ ) of the  $\Lambda$ -doublet. The term

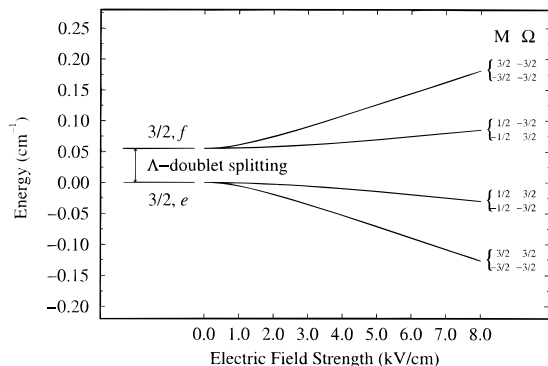


**Figure 1.** Graphic representation of the Stark effect in the lowest  $\Lambda$ -doublet of OH. Each Stark state is labeled with  $M$  and  $\Omega$ , see the text.

$\Delta E_\Lambda$  denotes the splitting between the doublet states in zero field. Diagonalization yields for the eigenvalues:

$$\lambda_f(E) = \frac{1}{2}\Delta E_\Lambda \left( 1 + \sqrt{1 + \left( \frac{2Q}{\Delta E_\Lambda} \right)^2} \right) \quad (11)$$

$$\lambda_e(E) = \frac{1}{2}\Delta E_\Lambda \left( 1 - \sqrt{1 + \left( \frac{2Q}{\Delta E_\Lambda} \right)^2} \right) \quad (12)$$

In Figure 1 the Stark splitting for the  $J = 3/2$  ground state is drawn as a function of the electric field strength. As can be seen, the effect starts nonlinear, but for high fields (i.e., when the Stark shift is in the order of the  $\Lambda$ -doublet splitting) a linear dependence on the field strength can be observed.

The electric field not only shifts and splits the energy levels of the molecule, but it also orients the dipole moment of the molecule in space. Classically, the molecule will prefer the configuration of minimum energy, which means that the dipole moment will be oriented parallel to the electric field. Quantum mechanically, the wave function of the molecule will change which determines the physical orientation of the molecule in space.

The field dependent eigenfunctions, denoted with  $\tilde{\Psi}_e$ , corresponding to the eigenvalues  $\lambda_e$ , of the  $2 \times 2$  matrix as defined in eq 10 can be expressed in the field free eigenfunctions (eq 4) as

$$\tilde{\Psi}_f(\Omega, J, M; E) = \alpha_f(E)\Psi_f(\Omega, J, M) + \beta_f(E)\Psi_e(\Omega, J, M) \quad (13)$$

$$\tilde{\Psi}_e(\Omega, J, M; E) = \alpha_e(E)\Psi_f(\Omega, J, M) + \beta_e(E)\Psi_e(\Omega, J, M) \quad (14)$$

Substitution of these eigenfunctions in eq 10 results in the following relations

$$\beta_f = \frac{\lambda_f - \Delta E_\Lambda}{Q} \alpha_f = \frac{1}{2} \frac{-\Delta E_\Lambda + \sqrt{\Delta E_\Lambda^2 + 4Q^2}}{Q} \alpha_f \quad (15)$$

$$\beta_e = \frac{\lambda_e - \Delta E_\Lambda}{Q} \alpha_e = \frac{1}{2} \frac{-\Delta E_\Lambda - \sqrt{\Delta E_\Lambda^2 + 4Q^2}}{Q} \alpha_e \quad (16)$$

In the high field limit, where  $Q \gg \Delta E_\Lambda$ , this reduces to

$$\beta_f = \frac{|Q|}{Q} \alpha_f = \frac{|M|}{-M} \alpha_f \quad (17)$$

$$\beta_e = \frac{-|Q|}{Q} \alpha_e = \frac{|M|}{M} \alpha_e \quad (18)$$

To gain insight in the orientation of the molecule with regard

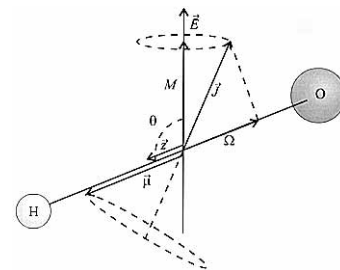


**Figure 2.** Picture of the vector representation of the quantum mechanical quantities that play a role when describing the effects of an electric field on the OH molecule. The intermolecular axis ( $\hat{z}$ ) is chosen in the direction of the dipole moment, pointing from the O atom toward the H atom. The picture drawn is for a combination of negative  $\Omega$  and positive  $M$  for a wave function of f-symmetry. This results in an average orientation of the oxygen side of the molecule along the direction of the  $\vec{E}$ -field. This is also the state which is selected in the hexapole.

to the electric field, the wave functions as defined in eqs 13 and 14 are evaluated. For simplicity the intermediate character of OH is neglected ( $C_1 = 0$  and  $C_2 = 1$  for the  $\Omega = 3/2$  ladder). When normalizing the wave functions and using the expressions for  $\Psi_e$  as given in eqs 3 and 4, it then follows, still in the high field limit,

$$\Psi_f(\Omega, J, M; \infty) = \begin{cases} |\Omega JM\rangle & \text{if } M < 0 \\ |-\Omega JM\rangle & \text{if } M > 0 \end{cases} \quad (19)$$

$$\Psi_e(\Omega, J, M; \infty) = \begin{cases} |-\Omega JM\rangle & \text{if } M < 0 \\ |\Omega JM\rangle & \text{if } M > 0 \end{cases} \quad (20)$$

From the initially chosen convention with regard to the sign of  $\Omega$  for the case (a) wave functions (eq 2), it can be seen that, for  $|\Omega JM\rangle$ , the molecule is oriented with the H-end in the direction of  $\vec{J}$ . For  $|-\Omega JM\rangle$  it is oriented the other way around. When combining this with the orientation of  $\vec{J}$  with respect to  $\vec{E}$ , given by  $M$ , one can see that  $\tilde{\Psi}_f$  describes a molecule with an average orientation of the O-end in the direction of the electric field whereas  $\tilde{\Psi}_e$  describes a molecule with an average orientation of the H-end in the direction of the electric field. In Figure 2 a vector representation of this situation is drawn for the case of  $\tilde{\Psi}_f$  with  $M > 0$ .

The eigenfunctions follow from eqs 15 and 16 for the  $\alpha$  and  $\beta$  constants:

$$\alpha^2 \equiv \alpha_f^2 = \beta_e^2 = \frac{1}{2} + \frac{1}{2\sqrt{1 + \left( \frac{2Q}{\Delta E_\Lambda} \right)^2}} \quad (21)$$

$$\beta^2 \equiv \beta_f^2 = \alpha_e^2 = \frac{1}{2} - \frac{1}{2\sqrt{1 + \left( \frac{2Q}{\Delta E_\Lambda} \right)^2}} \quad (22)$$

When describing and interpreting a collision event with an oriented molecule, the average degree of orientation is one of the key quantities. This is a function of the electric field and the projection of  $\vec{J}$  onto the direction of the electric field ( $M$ ). Quantum mechanically, the induced orientation can be understood by evaluating the orientation distribution function. The orientation distribution function follows from the wave function describing the molecule in the electric field according to<sup>16</sup>

$$P_{\Omega JM}^e(\cos \theta) \sin \theta \, d\theta = \int \int \tilde{\Psi}_e^*(\Omega, J, M; E) \tilde{\Psi}_e(\Omega, J, M; E) \sin \theta \, d\theta \, d\phi \, d\psi \quad (23)$$

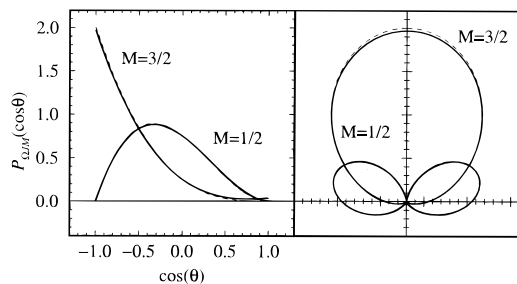


**Figure 3.** Orientational distribution of OH in the state  $|^{3/2, 3/2}M\rangle$ . The left hand side of the graph shows this distribution as a function of  $\theta$ , the right hand side of the graph shows a polar plot. The direction of the  $\vec{E}$ -field is chosen in the direction of the vertical axis of the polar plot. The solid line represents the orientation distribution function as present during the experiment (with  $\alpha = 0.794$ ), the dashed line represents the orientation distribution function in the high field limit with  $\alpha = 0.707$ .

in which the integration over  $\psi$  and  $\phi$  usually results in a factor  $4\pi^2$  since  $\Psi$  does not have a  $\psi$  or  $\phi$  dependence. The field dependent wave functions (eqs 13 and 14) consist of both an  $\Omega = 3/2$  and an  $\Omega = 1/2$  part, according to eq 3. For the relevant  $J = 3/2$ ,  $\Omega = 3/2$  state, however, it would complicate the following calculation unnecessarily when incorporating the slight  $\Omega = 1/2$  character ( $C_1^2 \approx 0.030$ ). Instead, we assume that  $C_1 = 0$  and  $C_2 = 1$ . It then follows for the  $3/2$  f state

$$P_{3/2, 3/2 M}^f(\cos \theta) = \left(\frac{\alpha + \beta}{\sqrt{2}}\right)^2 \int \int \Phi^*(^{3/2, 3/2, M}) \Phi(^{3/2, 3/2, M}) d\phi d\psi + \left(\frac{\alpha - \beta}{\sqrt{2}}\right)^2 \int \int \Phi^*(-^{3/2, 3/2, M}) \Phi(-^{3/2, 3/2, M}) d\phi d\psi \quad (24)$$

with the field independent wave functions  $\Phi(\Omega, J, M)$  given by eq 1. When dropping the  $|\Lambda\Sigma\rangle$  part of eq 1 and writing the  $\mathcal{D}$ -functions<sup>12</sup> as

$$\mathcal{D}_{\Omega M}^J(\phi, \theta, \psi) = e^{-i\phi\Omega} d_{\Omega M}^J(\theta) e^{-i\psi M} \quad (25)$$

the orientation distribution function becomes

$$P_{3/2, 3/2 M}^f(\cos \theta) = ((\alpha + \beta)d_{3/2 M}^{3/2})^2 + ((\alpha - \beta)d_{-3/2 M}^{3/2})^2 \quad (26)$$

A convenient table of the  $d$ -functions can be found in ref 12, from which it follows for the rotational ground state and positive values of  $M$ ,

$$P_{3/2, 3/2, 3/2}^f(\cos \theta) = (\alpha + \beta)^2 \cos^6\left(\frac{\theta}{2}\right) + (\alpha - \beta)^2 \sin^6\left(\frac{\theta}{2}\right) \quad (27)$$

$$P_{3/2, 3/2, 1/2}^f(\cos \theta) = (\alpha + \beta)^2 3 \cos^4\left(\frac{\theta}{2}\right) \sin^2\left(\frac{\theta}{2}\right) + (\alpha - \beta)^2 3 \cos^2\left(\frac{\theta}{2}\right) \sin^4\left(\frac{\theta}{2}\right) \quad (28)$$

Note that, for positive values of  $M$ , according to eqs 17, 21, and 22, the relation between  $\alpha$  and  $\beta$  is given by  $\beta = -\sqrt{1 - \alpha^2}$ . A plot of these functions is given in Figure 3 for  $\alpha = 1/\sqrt{2}$  (high field limit) and for the value of  $\alpha = 0.794$  as has been realized in the present collision experiment. One can see from Figure 3 that for realistic fields the resulting orientation distribution function is very close to the high field limit. The average orientation for the  $M = 3/2$  state is much closer to  $\theta =$

**TABLE 1: Legendre Expansion Coefficients As Defined in Eq 31**

$ \Omega JM\rangle$	$C_0$	$C_1$	$C_2$	$C_3$
$1/2, 1/2, 1/2$	$1/2$	$1/2$		
$3/2, 3/2, 3/2$	$1/4$	$9/20$	$1/4$	$1/20$
$3/2, 3/2, 1/2$	$1/4$	$3/20$	$-1/4$	$-3/20$

0 than for the  $M = 1/2$  state. The average orientation can be calculated by evaluating

$$\begin{aligned} \langle \cos \theta \rangle &= \int P_{\Omega JM} \cos \theta \sin \theta d\theta \\ &= 2\alpha\beta \frac{\Omega M}{J(J+1)} \end{aligned} \quad (29)$$

The maximum value of the average orientation is obtained for  $\alpha = -\beta = 1/2\sqrt{2}$ , which results in  $\langle \cos \theta \rangle_{\max} = 3/5$  for the  $M = 3/2$  state and only  $1/5$  for the  $M = 1/2$  state. The relative population of the  $M$ -states in the collision area is therefore of large influence on the total orientation distribution function in the collision area. Knowledge of these relative populations is thus required to be able to interpret the collisional results correctly.

The orientation distribution function can also be expressed as an expansion in Legendre polynomials  $P_n(\cos \theta)$ , which is particularly convenient when theoretically deriving cross sections<sup>17</sup>

$$P_{\Omega JM}(\cos \theta) = \frac{2J+1}{2} \sum_{n=0}^{2J} C_n(\Omega JM) P_n(\cos \theta) \quad (30)$$

At the present conditions, to a good approximation the real orientation distribution function may be set equal to the orientation distribution function in the high field limit, as can be seen from Figure 3. The assumption is therefore made that  $\alpha = -\beta = 1/2\sqrt{2}$ . In this case the constants  $C_n$  are given by<sup>16</sup>

$$C_n = (2n+1)(-1)^{M-\Omega} \begin{pmatrix} J & J & n \\ \Omega & -\Omega & 0 \end{pmatrix} \begin{pmatrix} J & J & n \\ M & -M & 0 \end{pmatrix} \quad (31)$$

In Table 1 these coefficients are given for the relevant values of  $\Omega$ ,  $J$ , and  $M$ .

**2.2. LIF Spectroscopy of OH in an Electric Field.** The OH molecules are probed via LIF spectroscopy of the  $\Sigma \leftarrow \Pi$  band at 308 nm. Without the presence of an electric field, no external axis is defined and thus each state will be degenerate in  $M$ . The linestrength of each transition will then be given by the sum over all allowed  $\Delta M$  transitions, yielding a spherical radiation pattern of the total fluorescence, when all fluorescence pathways are taken into account.

In an electric field, this picture changes. In this case the electric field lifts the degeneracy of each rotational level and allows only specific  $M' \leftarrow M''$  transitions. These transitions exhibit a dependence on the polarization of the excitation radiation and have a  $\Delta M$  dependent nonspherical radiation pattern in space. Because the detection optics can image only radiation within a certain solid angle onto the photomultiplier, the  $\Delta M = 0$  transitions will have a different detection efficiency than the  $\Delta M = \pm 1$  transitions. In general, this implies that the various rotational states are detected with a different efficiency, which is also polarization dependent.

A second effect introduced by the electric field is the mixing of the parity of the  $\Lambda$ -doublet states. This mixing causes a

change in linestrengths and gives rise to transitions which are not allowed without the electric field.

In this section it will be shown that the effects described above can be used to experimentally determine the orientation distribution function and the ratio of the populations of the  $M = 1/2$  and  $M = 3/2$  substates in the beam focused by the hexapole.

The linestrength of a transition in the  $A \leftarrow X$  band of OH is given by

$$\begin{aligned} \mathcal{L}_{i,j} = & |\langle C_1 \Psi_e(1/2, J, M) | \sum_v \tilde{u}_q^{(1)} \mathcal{D}_{vq}^{(1)} |^2 \Sigma_{1/2}^+, J', M', p' \rangle + \\ & \langle C_2 \Psi_e(3/2, J, M) | \sum_v \tilde{u}_q^{(1)} \mathcal{D}_{vq}^{(1)} |^2 \Sigma_{1/2}^+, J', M', p' \rangle |^2 \quad (32) \end{aligned}$$

In this equation, the ket  $|\Sigma\rangle$  represents the wave function of the first electronic excited state and  $p'$  the parity of this state. The body-fixed coordinate  $q = 0$  corresponds with a polarization of the light parallel to the electric field, and  $q = \pm 1$  corresponds to a perpendicular orientation of the polarization. This integral can be split into a part including the  $J$  and  $M$  dependence and a part which is independent of  $J$  and  $M$ . When disregarding the  $J$ -independent part, the integral can be written as

$$\begin{aligned} \mathcal{L}_{i,j} \propto & \left\{ C_2 \begin{pmatrix} J & 1 & J' \\ -3/2 & 1 & 1/2 \end{pmatrix} \pm \right. \\ & \left. C_1 \begin{pmatrix} J & 1 & J' \\ -1/2 & 1 & -1/2 \end{pmatrix} \right\}^2 (2J+1)^2 \begin{pmatrix} J & 1 & J' \\ -M & q & M' \end{pmatrix}^2 \quad (33) \end{aligned}$$

In the absence of an electric field, one has to sum over  $q$  and  $M'$ , resulting in a contribution of the last  $3J$ -symbol to be equal to 1.<sup>18</sup> With an electric field, however, the last  $3J$ -symbol is responsible for the steric dependence of the line strength:<sup>19</sup>

$$\mathcal{L}_{i,j}(\vartheta) \propto \begin{cases} 1/2(1 + \cos^2 \vartheta) & \text{for } \Delta M = \pm 1, \quad q = \mp 1 \\ \sin^2 \vartheta & \text{for } \Delta M = 0, \quad q = 0 \end{cases} \quad (34)$$

with  $\vartheta$  the angle between the direction of the radiation and the quantization axis *i.e.*, the electric field axis. This applies both to excitation and to fluorescence. In the present experiment the effect in excitation is generally negligible, because of saturation effects, but in fluorescence it plays a role. Because the detector can only see radiation within a certain solid angle, the detection efficiency of radiation from a parallel transition in emission or a perpendicular transition is different. As in a parallel excitation a different set of  $M$ -substates is populated than in a perpendicular excitation, the fluorescence for both ways of excitation will encompass a different  $\vartheta$ -dependence. This has to be taken into account in the interpretation of the LIF results.

The parity mixing of the  $\Lambda$ -doublet states by the electric field is given by the wave functions as described in eqs 13 and 14. This mixing enables certain "forbidden" transitions. In the present experiment, the hexapole state selection results in a nearly pure beam of OH in the  $3/2, f$  state. The  $P_1(1)$  transition to the  $J = 1/2$  state is almost completely suppressed because this transition starts from the  $3/2, e$  state, which has only a few percent population. The mixing of both  $\Lambda$ -doublet states, however, introduces another transition, namely, the one starting from the  $3/2, f$  state to the same upper level as in the  $P_1(1)$  transition,  $J' = 1/2, p' = +$ . This new line, denoted with  $P'_1(1)$ , is frequency shifted with respect to the  $P_1(1)$  by a small amount given by the  $\Lambda$ -doubling in the lowest rotational level and the Stark shift of the  $3/2, f$  state. The intensity of this line

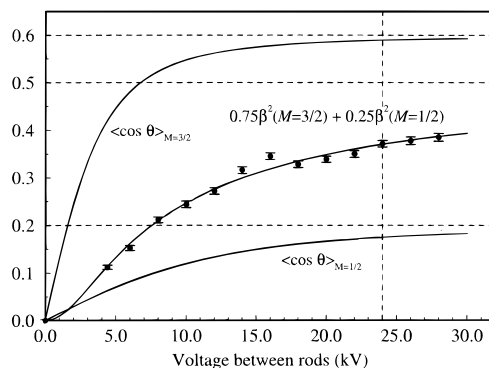


**Figure 4.** The mixing of the  $M$  substates of the  $J = 3/2$   $\Lambda$ -doublet of OH( ${}^2\Pi_{3/2}, \nu = 0$ ). The middle curve represents a theoretical fit to the experimental LIF intensity (dots) of the  $P'_1(1)$  transition. The upper curve represents the value of the average orientation  $\langle \cos \theta \rangle$  for  $M = 3/2$ , with  $\theta$  the angle between the internuclear axis and the  $E$ -field. The lower curve is for  $M = 1/2$ . In the collision experiment a voltage of 24 kV between the rods was used, which is indicated by the dashed vertical line.

is a direct function of the mixing and enters the line strength as

$$\begin{aligned} \mathcal{L} \propto & |\langle \tilde{\Psi}_f(3/2, 3/2, M; E) | \sum_v \tilde{u}_q^{(1)} \mathcal{D}_{vq}^{(1)} |^2 \Sigma_{1/2}^+, 1/2, M', p' \rangle|^2 \propto \\ & |\alpha \langle \Psi_f(3/2, 3/2, M) | \sum_v \tilde{u}_q^{(1)} \mathcal{D}_{vq}^{(1)} |^2 \Sigma_{1/2}^+, 1/2, M', p' \rangle + \\ & \beta \langle \Psi_e(3/2, 3/2, M) | \sum_v \tilde{u}_q^{(1)} \mathcal{D}_{vq}^{(1)} |^2 \Sigma_{1/2}^+, 1/2, M', p' \rangle|^2 \propto \\ & \beta^2 |\langle \Psi_e(3/2, 3/2, M) | \sum_v \tilde{u}_q^{(1)} \mathcal{D}_{vq}^{(1)} |^2 \Sigma_{1/2}^+, 1/2, M', p' \rangle|^2 \quad (35) \end{aligned}$$

It should be noted that the  $|\Sigma_{1/2}^+, J, M, p\rangle$  states are not influenced by the electric field to first order. The influence of the electric field on the linestrength of the  $P'_1(1)$  transition is thus given by the  $\beta^2$  factor (eq 22). The important implication of this result is that the field dependence of the intensity of the  $P'_1(1)$  transition provides direct information about the orientation distribution function which is determined by  $\alpha$  and  $\beta$ .

The  $P'_1(1)$  transition exhibits also another property. It follows from eq 33 that with a parallel  $P_1(1)$  transition one can only excite molecules having  $M = 1/2$ , whereas with a perpendicular transition, both  $M$ -states are probed. Consequently, a measurement of the polarization dependence of the  $P'_1(1)$  transition yields direct information about the ratio of the number of molecules in the  $M = 1/2$  and  $3/2$  states. The interpretation of the polarization effect is simplified by the fact that both for parallel and perpendicular excitation, the same  $M$ -levels ( $M = \pm 1/2$ ) are reached in the upper state. This implies that there is no difference in detection efficiency for both ways of excitation. Because in our experiment the laser power used is high enough to saturate the transitions, the relation between the polarization dependence and the number densities of molecules in the different  $M$ -levels in the lowest rotational state, is straightforward:

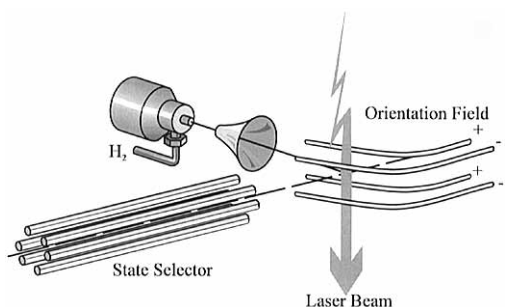
$$\frac{n_{3/2}}{n_{1/2}} = \frac{I_{\perp} - I_{\parallel}}{I_{\parallel}} \quad (36)$$

with  $I_{\perp}$  and  $I_{\parallel}$  denoting the LIF intensity for perpendicular and parallel excitation, respectively.

In Figure 4 the field dependence of the  $P'_1(1)$  transition is pictured. Through the measured points a fit of the theoretical curve is drawn. Because of the focusing properties of the hexapole, both molecules with  $M_j = 1/2$  and  $M_j = 3/2$  are present. Via the polarization dependence of the  $P'_1(1)$  transition the

**TABLE 2: Mixing and (Possible) Average Orientation of All Experimentally Relevant States of OH at the Electric Field Strength Employed during the Experiment**

$\Omega = 3/2$				$\Omega = 1/2$			
$J, M$	$\beta(24 \text{ kV})$	$\langle \cos \theta \rangle$	$\langle \cos \theta \rangle_{\text{max}}$	$J, M$	$\beta(24 \text{ kV})$	$\langle \cos \theta \rangle$	$\langle \cos \theta \rangle_{\text{max}}$
$3/2, 1/2$	0.5059	0.1746	0.2000	$1/2, 1/2$	0.3900	0.2394	0.3333
$3/2, 3/2$	0.6390	0.5898	0.6000	$3/2, 1/2$	0.0626	0.0083	0.0667
$5/2, 1/2$	0.1031	0.0176	0.0857	$3/2, 3/2$	0.1797	0.0707	0.2000
$5/2, 3/2$	0.2769	0.1368	0.2571	$5/2, 1/2$	0.0257	0.0015	0.0571
$5/2, 5/2$	0.3934	0.3100	0.4286	$5/2, 3/2$	0.0765	0.0131	0.1714
$7/2, 1/2$	0.0261	0.0025	0.0476	$5/2, 5/2$	0.1256	0.0356	0.2857
$7/2, 3/2$	0.0777	0.0221	0.1429				
$7/2, 5/2$	0.1274	0.0602	0.2381				
$7/2, 7/2$	0.1744	0.1145	0.3333				
$9/2, 1/2$	0.0094	0.0006	0.0303				
$9/2, 3/2$	0.0281	0.0051	0.0909				
$9/2, 5/2$	0.0467	0.0141	0.1515				
$9/2, 7/2$	0.0652	0.0276	0.2121				
$9/2, 9/2$	0.0835	0.0454	0.2727				

**Figure 5.** Detail view of the setup showing the placement of the rods producing the orientation field.

ratio of the two  $M$ -states was determined as  $n_{3/2}/n_{1/2} = 3.0 \pm 0.1$ . The field dependence of the fluorescence is then given by

$$\angle(E) \propto 0.75\beta^2(M = 3/2, E) + 0.25\beta^2(M = 1/2, E) \quad (37)$$

The fitted curve for  $\angle$  in Figure 4 is based on this expression. Two parameters were determined by the fit. One is a proportionality constant which relates the LIF intensity to the linestrength, the other one is a factor relating the actual electric field to the voltage difference between the rods.

Also pictured are the averages of  $\langle \cos \theta \rangle$  for molecules in both the  $M = 3/2$  and  $1/2$  states. As can be seen for  $M = 3/2$ ,  $\langle \cos \theta \rangle$  approaches the maximum attainable value much faster than the mixing of the  $\Lambda$ -doublet states does. This is advantageous because a moderate field strength can be applied which yields an excellent orientation in the prepared state without introducing a strong mixing. Possible symmetry effects in the collisional cross section would be concealed when the mixing is too strong. In Table 2 an overview is given for the mixing and averaged orientation of all states which are accessible with our collision energies. One can see that only the  $\Omega = 3/2, J = 5/2$ , and the  $\Omega = 1/2, J = 1/2$  states show a significant amount of  $\Lambda$ -doublet mixing in the field which is employed during the experiment. When theoretically describing oriented collisions in an electric field this mixing of the excited state has to be taken into account.<sup>17</sup>

### 3. Experimental Section

**3.1. Setup.** A detailed description of the crossed molecular beam setup without orientation field is given in refs 6 and 7 and will not be repeated here. A schematic view of the collision zone with orientation field is given in Figure 5. The OH molecules are state selected by an electrostatic hexapole and subsequently oriented in an electric field. The beam of oriented

molecules is crossed under right angles with a secondary beam. In the region where the two beams overlap, the rotational excitation of the OH molecule is studied via LIF spectroscopy. As collision partners are used He, Ar,  $n$ -H<sub>2</sub> and  $p$ -H<sub>2</sub>. The  $p$ -H<sub>2</sub> is prepared on line during the experiment as described in ref 7. The collision energies involved are 394 cm<sup>-1</sup> for He, 451 cm<sup>-1</sup> for Ar, and 596 cm<sup>-1</sup> for both H<sub>2</sub> species.

The orientation field is produced by four stainless steel rods which are set pairwise on a potential difference of 24 kV. The distance between the pairs is 18 mm. This arrangement was chosen because the probe region has to be accessible from six directions: two molecular beams and a laser beam. The field produced in this way is not perfectly homogeneous, but when only taking into account the region where the molecules are scattered and detected, calculations based on a geometry of four infinitely long rods show that the field is very close to homogeneous. With respect to a flat plate capacitor geometry the field strength is reduced by a factor 1.47, which is in good agreement with the observations (see later). In the immediate neighbourhood of the orientation rods some grounded metal parts are present. To minimize their distortion to the field, one pair of rods is held at a negative voltage, the other pair is held at a positive voltage. The resulting potential in the scattering region is then close to zero, and a reversal of the voltages will have little effect on the field strength. As a check for this invariance, the effective field at the probe area was determined via the  $P'_1(1)$  transition, as outlined in section 2.2. When the field was reversed, the intensity of this line remained unchanged within the experimental accuracy. The direction of the field can be reversed by exchanging the connection of the power supplies to the rods. Two other checks were performed to assure that the orientation device did not have deviations from the desired behavior. Both were performed after reconnecting the wires to the rods in a way that the field is perpendicular to the plane formed by the two crossing molecular beams. First, the polarization dependence of the intensity of the  $P'_1(1)$  was checked. No polarization dependence was found within the experimental accuracy, which is to be expected. Secondly, for several transitions the collision induced signal with the electric field pointing upwards was compared to the signal with the electric field pointing downwards. Also in this case the signals corresponded to each other within the experimental accuracy. From both tests it can be concluded that the electric field in the collision area points in the direction for which the orientation device has been designed.

One of the design problems in this setup is the suppression of the stray light of the laser beam which is scattered by the rods. As the observed fluorescence radiation is resonant with

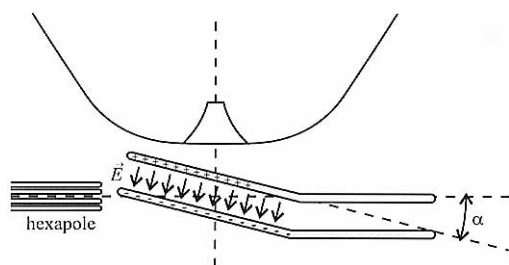


**Figure 6.** Sketch of the geometry of the orientation device, showing the definition of the angle  $\alpha$ . The angle drawn is  $14^\circ$  which corresponds to  $\text{H}_2$  collisions.

the excitation wavelength, this stray light cannot be removed by using a filter. Adequate shielding of the stray light was obtained by covering the rods as seen by the photomultiplier using black paper.

The LIF detection was slightly modified with respect to the setup used previously, because in this experiment the polarization of the laser plays an important role. To have control over the polarization a UV transparent Glan–Taylor prism is used to linearly polarize the laser beam, and a zero order  $1/2\lambda$ -plate for 308 nm is used to enable rotation of the polarization. The polarizing optics is inserted in front of the entrance window of the vacuum chamber. Polarization distortion by the window is avoided by using a quartz plate which is thick enough with respect to its diameter to resist the pressure difference between the inside and the outside of the chamber without deformation.

**3.2. Initial State Preparation and Orientation.** In the hexapole molecules in the upper  $\Lambda$ -doublet states of each rotational level are focused and molecules in the lower  $\Lambda$ -doublet states are defocused. The focusing is based on the Stark effect and consequently every  $J, M$  state will exhibit a different focusing behavior. The hexapole geometry and voltage is optimized for focusing molecules in the  $J = 3/2, M = 3/2$  state. In this setup the beam is focused twice, once halfway the hexapole and a second time a few centimeters behind the exit of the hexapole. Although molecules in the  $3/2, 1/2$  state are focused less tightly, there is still a fair amount of  $M = 1/2$  molecules present in the collision center. By varying the polarization of the laser when exciting the  $P'_1(1)$  transition, as outlined in section 2.2, the ratio of the population of  $M = 3/2$  and  $M = 1/2$  is found to be  $3.0 \pm 0.1$  for the  $\Omega = 3/2, J = 3/2$  state. Also a small amount of  $J = 5/2$  is present, but the total population of this rotational level is only 6% of the population in the  $J = 3/2$  state.

In Figure 6 the geometry of the orientation field is sketched. The angle  $\alpha$  is defined as the angle between the axis of the secondary beam and the direction of the electric field. The direction of the electric field is chosen to be parallel with the relative velocity vector. This results in  $\alpha = 14^\circ$  for  $n$ - and  $p$ - $\text{H}_2$ ,  $45^\circ$  for Ar, and  $23^\circ$  for He. In the setup as drawn in Figure 6 the OH molecule is oriented with the H-end toward the secondary beam molecules. The effective field as measured via the  $P'_1(1)$  transition is  $8.8 \pm 0.1$  kV/cm at a potential difference of 24 kV. This corresponds to the scale used in Figure 4. The derived fieldstrength is in good agreement with the calculated value of 9.1 kV/cm. The average orientation  $\langle \cos \theta \rangle$  of the OH molecules at the applied voltage of 24 kV is very close to  $\langle \cos \theta \rangle_{\text{max}}$ , as can be seen in Table 2. When an ideal orientation is assumed, and both the  $M = 3/2$  and  $M = 1/2$  states are taken into account, then the total (i.e., both  $M$ -states together) orientational distribution function of OH can, according

to eq 3 of ref 20 and eq 30 be expressed as

$$P(\cos \theta) = 0.25P_0(\cos \theta) + 0.375P_1(\cos \theta) + 0.125P_2(\cos \theta) \quad (38)$$

The angle  $\theta$  is the angle between the internuclear axis of the OH molecule and the electric field vector. The term with  $n = 3$  vanishes because the contribution of the  $M = 3/2$  state accidentally cancels the contribution of the  $M = 1/2$  state.

The distance between the orientation device and the hexapole is a few millimeter, resulting in a continuously present electric field along the beam path. No extra guiding field has to be applied to ensure a conservation of the coupling between the focused molecules and the electric field. When this coupling would be lost, also the orientation would be lost, resulting in a net alignment, and consequently no effect of the electric field reversal on the cross sections would be observable.

**3.3. Data Reduction.** The collisionally induced rotational excitation of OH is probed state selectively in several consecutive measurements. The relative population transfer from the initial state to an excited state is probed via LIF spectroscopy, as described in refs 6 and 7. The measured LIF intensity is a linear measure for the number of excited molecules, from which the cross section for the rotational transition can be derived. Due to saturation the relative state-to-state cross sections are directly obtained from the relative LIF intensities.

The effect of the orientation on the cross section was determined by measuring the steric asymmetry factor:

$$S = \frac{I_{\text{HO-X}} - I_{\text{OH-X}}}{I_{\text{HO-X}} + I_{\text{OH-X}}} \quad (39)$$

where  $I_{\text{HO-X}}$  denotes the LIF intensity as measured with the O-end in the direction of the collision partner X, and  $I_{\text{OH-X}}$  denotes the reverse orientation. The LIF intensity for both orientations is measured in one experiment, by only changing the direction of the electric field. The weighted average of 6 of these measurements is then used to construct the final value. The LIF intensity which is measured for a particular transition is influenced by the polarization which is chosen for the excitation. Depending on the polarization a different set of  $M$ -levels in the excited state is populated. The fluorescence is a sum of both  $\Delta M = \pm 1$  and  $\Delta M = 0$  transitions which are, according to eq 34 detected with a different efficiency. Every  $M$ -level in the excited state will have a unique distribution across  $\Delta M = \pm 1$  and  $\Delta M = 0$  transitions and, hence, will be detected with a specific efficiency, depending on the direction of the polarization of the laser. This detection efficiency, however, is a common factor in  $I_{\text{HO-X}}$  and  $I_{\text{OH-X}}$  which cancels by definition in the steric asymmetry factor (eq 39), provided the polarization is the same in the measurement of both  $I_{\text{HO-X}}$  and  $I_{\text{OH-X}}$ . There is, henceforth, no influence of the polarization on the steric asymmetry factor. In practice, the polarization is chosen which yields the highest LIF intensity, in order to have the highest signal-to-noise ratio.

#### 4. Results and Discussion

In Table 3 the steric asymmetry factors for rotational excitation of OH induced by collisions with He, Ar,  $p$ - $\text{H}_2$ , and  $n$ - $\text{H}_2$  are presented. Some transitions, although within reach of the collision energy, have a very small cross section and hence also a large relative statistical error in the steric asymmetry factor. Due to this large error the steric asymmetry factor becomes almost meaningless for these transitions, and they are thus not included in Table 3. The presented data include the

**TABLE 3: Steric Asymmetry Factor  $S$  for Rotational Excitation of Oriented OH ( ${}^2\Pi_{3/2}$ ,  $J = {}^3/2$ )<sup>a</sup>**

final state			collision partner			
$\Omega$	$J$	$\epsilon$	He	$p$ -H <sub>2</sub>	$n$ -H <sub>2</sub>	Ar
${}^{3/2}$	${}^{5/2}$	f	-0.18 ± 0.13	0.07 ± 0.03	0.07 ± 0.02	0.16 ± 0.06
	${}^{5/2}$	e	-0.13 ± 0.02	0.05 ± 0.01	0.00 ± 0.02	0.00 ± 0.02
	${}^{7/2}$	f	-0.08 ± 0.31	-0.08 ± 0.07	-0.17 ± 0.08	-0.17 ± 0.17
${}^{1/2}$	${}^{7/2}$	e	-0.27 ± 0.03	-0.04 ± 0.02	-0.11 ± 0.02	-0.13 ± 0.04
	${}^{1/2}$	f	-0.06 ± 0.02	0.04 ± 0.02	0.04 ± 0.02	0.05 ± 0.11
	${}^{1/2}$	e	-0.05 ± 0.01	0.00 ± 0.02	0.01 ± 0.01	
	${}^{3/2}$	f	-0.06 ± 0.03	-0.07 ± 0.02	-0.03 ± 0.02	
	${}^{3/2}$	e	-0.01 ± 0.03	0.01 ± 0.02	-0.02 ± 0.01	
$E_{\text{coll}}$ (cm <sup>-1</sup> )			394	596	596	451

<sup>a</sup> Negative value means preference for excitation via collisions on the H-end; Positive value means a preference for O-end excitation.

steric asymmetry factor for transitions to the  $J = {}^{5/2}$  and  ${}^{7/2}$  states in the  $\Omega = {}^{3/2}$  ladder and the  $J = {}^{1/2}$  and  ${}^{3/2}$  states in the  $\Omega = {}^{1/2}$  ladder. It can be concluded from Table 3 that for all scattering gases the steric asymmetries are very small, but non-zero, for the multiplet changing transitions.

For He there is a consistent preference for excitation at the H-end of OH. The strongest asymmetry in He collisions is observed for the transition to the  ${}^{7/2}$ , e state. The other molecules show a preference for excitation at the O-end for transitions to the  ${}^{3/2}$ ,  ${}^{5/2}$  and  ${}^{1/2}$ ,  ${}^{1/2}$  states and a preference for excitation at the H-end for transitions to the  ${}^{3/2}$ ,  ${}^{7/2}$  and  ${}^{1/2}$ ,  ${}^{3/2}$  states.

With respect to nonoriented scattering the state-to-state cross sections for collisions with  $p$ -H<sub>2</sub> ( $J = 0$ ) show the same rotational dependence as for He.<sup>7</sup> The observed differences between He and  $p$ -H<sub>2</sub> scattering involve mainly the  $\Lambda$ -doublet transition and can be attributed to the presence of  $p$ -H<sub>2</sub> ( $J = 2$ ) in the beam. The observed steric effects, however, are strongly different from each other. Possibly the presence of H<sub>2</sub> ( $J > 0$ ) molecules has a larger influence on the steric asymmetry than on the orientation averaged state-to-state cross sections themselves. This explanation is consistent with the observation that there is little difference between the effects observed for  $n$ -H<sub>2</sub> and  $p$ -H<sub>2</sub>. Ar shows more or less the same behavior as  $n$ -H<sub>2</sub>, which corresponds to the similarity in the relative magnitudes of the orientation averaged state-to-state cross sections.<sup>6,7</sup>

In general, when looking at the  $J$ -dependence of the steric effect, the trend is that for higher  $J$ -values of the excited state, the preference is more toward excitation at the H-end of OH, which is to be expected from a classical point of view. Because the O atom is situated very close to the center of mass, the probability for rotational excitation when the H-atom is hit, will be larger than when the O atom is hit. In the classical picture, the excitation of high  $J$ -states occurs at larger impact parameters, and hence the long-range part of the interaction potential plays a more important role. This long range part shows normally a smaller asymmetry than the short-range part of the potential. This rationale then leads to the conclusion that the steric asymmetry factor will approach zero when higher excitations play a role. The present sensitivity and collision energy do not allow us to measure this factor reliably for the higher  $J$ -states, so unfortunately a check of the validity of this assumption has to await further experimental improvements. The observed strong differences in the steric asymmetry for different parity states in nearly all observed rotational transitions suggest, however, that quantum interference effects play an important role.

*Ab initio* potentials for the description of the interaction between OH and H<sub>2</sub> have been developed by Offer and Van Hemert<sup>21</sup> and by Miller *et al.*<sup>22</sup> Both calculations predict an attractive well at the H-end of OH for an orientation of H<sub>2</sub> perpendicular with respect to the internuclear axis of OH. Also

an attractive well at the O-end of the molecule is predicted for an orientation of the H<sub>2</sub> molecule parallel to the internuclear axis of OH. In both cases the well depth is calculated to be in the range 120–200 cm<sup>-1</sup>. A good understanding of the steric effects is therefore difficult to base on these potentials without performing the scattering calculations. When the difference in orientation of the H<sub>2</sub> molecule with respect to OH is disregarded for both ends of OH, the classical picture would predict that excitation at the H-end of OH is favored.

Potentials for the He and Ar systems have been developed by Degli Esposti *et al.*<sup>23</sup> Quantum calculations of the state-to-state cross sections based on these potentials yielded an excellent agreement with our previous results on nonoriented scattering.<sup>6</sup> The potential surfaces for the two OH orientations show a larger anisotropy for Ar than for He. This seems to be in direct contradiction with our observation that He shows on the average larger steric asymmetry factors, whereas the state-to-state cross sections are smaller than for Ar. This discrepancy may be explained by the fact that Ar and He collisions are governed by different parts of the potential. Where for Ar the attractive part of the potential is dominating the collision process, for He it is more the repulsive part which is important. This different behavior is believed to be responsible also for the remarkably large difference between the observed  $\Lambda$ -doublet cross sections.<sup>23</sup> Due to the attractive potential, the OH molecule may first undergo a torque toward the Ar atom, whereby the original orientation is distorted. As a consequence the difference between the OH-Ar and HO-Ar orientations may be reduced causing a smaller steric asymmetry. This effect is expected to be the largest at small impact parameters, which might explain the difference in steric effects for the transition to the  $J = {}^{5/2}$  state in Ar and He collisions. Reorientation has been shown to be an important effect in scattering of Ca with methylhalides.<sup>24,25</sup> The low moment of inertia of OH is certainly in favor of this speculation. Quantum calculations based on the available *ab-initio* potentials for OH-Ar and OH-He should provide clarification.

In a similar experiment on inelastic scattering of oriented NO with Ar, Van Leuken *et al.*<sup>17</sup> found results which deviate quite strongly from our results. They found a strong symmetry dependence of the steric effect, where we observe a clear indifference toward the symmetry of the final state. The steric effects observed are not only much larger than the ones we observed, but also show a preference for excitation via the O-end of the molecule, where we see a preference for the other end. In their calculations performed on the NO-Ar system they obtained similar large and strong parity dependent effects, although the theoretical values did not correspond well to the experimental ones. The differences between OH and NO can partly be explained by the different character of both molecules. NO is a nearly pure Hund's case (a) molecule, where OH has a strong intermediate character. The case (a) character of NO



inhibits large quantum interferences and results in strong parity propensity rules in the inelastic cross sections.

## 5. Conclusions

In this experiment the steric asymmetry of the rotational energy transfer of OH scattered by He, Ar, *n*-H<sub>2</sub>, and *p*-H<sub>2</sub> is studied by measuring the cross sections for rotational excitation of oriented OH. The OH is oriented via hexapole state selection and application of a homogeneous electric field in the scattering area. This technique is shown to be a powerful way to achieve high degrees of orientation of OH. The orientation distribution function and the relative abundancies of the different *M*-components in the scattering center are verified experimentally via LIF techniques.

The results show that for He collisions, excitation of OH at the H-end is preferred above excitation at the O-end. This is also the case for collisions with Ar and H<sub>2</sub> except for transitions to the  $\Pi_{3/2}$ ,  $J = 5/2$  and  $\Pi_{1/2}$ ,  $J = 1/2$  states. Unfortunately the poor detection efficiency of the higher rotational states of OH inhibits a more profound study of the *J* dependence of the steric asymmetry. At this time no clear comparison with theory can be made, because of the lack of calculated cross sections for these oriented collisions. There are, however, *ab-initio* potentials available, which have been proven to give satisfying results for the description of nonoriented state-to-state cross sections. The present data allow for an even more stringent test of these potentials.

**Acknowledgment.** We thank Mr. E. van Leeuwen for his invaluable technical assistance and Dr. J. J. van Leuken and Prof. S. Stolte for their advice when we were starting this experiment.

## References and Notes

- (1) Toennies, J. P. *Farad. Discuss.* **1962**, 33, 96.
- (2) Kramer, K. H.; Bernstein, R. B. *J. Chem. Phys.* **1965**, 42, 767.

- (3) Parker, D. H.; Bernstein, R. B. *Annu. Rev. Phys. Chem.* **1989**, 40, 561.
- (4) Loesch, H. J.; Remscheid, A. *J. Chem. Phys.* **1990**, 93, 4779.
- (5) Harren, F.; Parker, D. H.; Stolte, S. *Comments At. Mol. Phys.* **1991**, 26, 109.
- (6) Schreel, K.; Schleipen, J.; Eppink, A.; Ter Meulen, J. J. *J. Chem. Phys.* **1993**, 99, 8713.
- (7) Schreel, K.; Ter Meulen, J. J. *J. Chem. Phys.* **1996**, 105, 4522.
- (8) Van Leuken, J. J. Ph.D. Thesis, Free University Amsterdam, Amsterdam, 1994.
- (9) Ghandi, S. R.; Curtiss, T. J.; Bernstein, R. B. *Phys. Rev. Lett.* **1987**, 59, 2951.
- (10) Mastenbroek, J. W. G.; Taatjes, C. A.; Nauta, K.; Janssen, M. H. M.; Stolte, S. *J. Phys. Chem.* **1995**, 99, 4360.
- (11) Meerts, W. L.; Dymanus, A. *Chem. Phys. Lett.* **1973**, 23, 45.
- (12) Zare, R. N. *Angular Momentum*; Wiley: New York, 1988.
- (13) Brown, J. M.; Hougen, J. T.; Huber, K. P.; Johns, J. W. C.; Kopp, I.; Lefebvre-Brion, H.; Merer, A. J.; Ramsay, D. A.; Rostas, J.; Zare, R. N. *J. Mol. Spectrosc.* **1975**, 55, 500.
- (14) Alexander, M. H.; Dagdigian, P. J. *J. Chem. Phys.* **1984**, 80, 4325.
- (15) Lefebvre-Brion, H.; Field, R. W. *Perturbations in the Spectra of Diatomic Molecules*; Academic: New York, 1986.
- (16) Choi, S. E.; Bernstein, R. B. *J. Chem. Phys.* **1986**, 85, 150.
- (17) Van Leuken, J. J.; Bulthuis, J.; Stolte, S.; Snijders, J. G. *Chem. Phys. Lett.* **1996**, 260, 595.
- (18) Edmonds, A. R. *Angular Momentum in Quantum Mechanics*; Princeton University Press: Princeton, NJ, 1957.
- (19) Demtröder, W. *Laser Spectroscopy*, 1st ed.; Springer Verlag: Berlin, 1981.
- (20) Choi, S. E.; Bernstein, R. B. *J. Chem. Phys.* **1985**, 83, 4463.
- (21) Offer, A. R.; Van Hemert, M. C. *J. Chem. Phys.* **1993**, 99, 3836.
- (22) Miller, S. M.; Clary, D. C.; Kliesch, A.; Werner, H.-J. *Mol. Phys.* **1994**, 83, 405.
- (23) Degli Esposti, A.; Berning, A.; Werner, H.-J. *J. Chem. Phys.* **1995**, 103, 2067.
- (24) Janssen, M. H. M.; Parker, D. H.; Stolte, S. *J. Phys. Chem.* **1996**, 100, 16072.
- (25) Meijer, A. J. H. M.; Groenenboom, G. C.; Van der Avoird, A. *J. Phys. Chem.* **1996**, 100, 16066.